**The EMBO Journal (2010) 29,** 1889–1902 | © 2010 European Molecular Biology Organization | All Rights Reserved 0261-4189/10
www.embojournal.org

THE EMBO JOURNAL

# Learning, AMPA receptor mobility and synaptic plasticity depend on n-cofilin-mediated actin dynamics

**Marco B Rust[1,2], Christine B Gurniak[1,3], Marianne Renner[4,5], Hugo Vara[6], Laura Morando[6], Andreas Görlich[2], Marco Sassoè-Pognetto[6], Mumna Al Banchaabouchi[1], Maurizio Giustetto[6], Antoine Triller[4], Daniel Choquet[5] and Walter Witke[1,3,*]**

[1]Mouse Biology Unit, European Molecular Biology Laboratory (EMBL), Monterotondo, Italy, [2]Department of Biology, Neurobiology/Neurophysiology Group, University of Kaiserslautern, Kaiserslautern, Germany, [3]Institute of Genetics, Rheinische Friedrich-Wilhelms University, Bonn, Germany, [4]Biologie Cellulaire de la Synapse N&P, INSERM U497, Ecole Normale Supérieure, Paris, France, [5]Physiologie Cellulaire de la Synapse, UMR 5091 CNRS/Université de Bordeaux, Bordeaux, France and [6]National Institute of Neuroscience Italy and Department of Anatomy, Pharmacology and Forensic Medicine, University of Turin, Turin, Italy

**Neuronal plasticity is an important process for learning, memory and complex behaviour. Rapid remodelling of the actin cytoskeleton in the postsynaptic compartment is thought to have an important function for synaptic plasticity. However, the actin-binding proteins involved and the molecular mechanisms that *in vivo* link actin dynamics to postsynaptic physiology are not well understood. Here, we show that the actin filament depolymerizing protein n-cofilin is controlling dendritic spine morphology and postsynaptic parameters such as late long-term potentiation and long-term depression. Loss of n-cofilin-mediated synaptic actin dynamics in the forebrain specifically leads to impairment of all types of associative learning, whereas exploratory learning is not affected. We provide evidence for a novel function of n-cofilin function in synaptic plasticity and in the control of extrasynaptic excitatory AMPA receptors diffusion. These results suggest a critical function of actin dynamics in associative learning and postsynaptic receptor availability.**

*The EMBO Journal* (2010) **29,** 1889–1902. doi:10.1038/emboj.2010.72; Published online 20 April 2010
*Subject Categories*: neuroscience; cell & tissue architecture
*Keywords*: actin cytoskeleton; neuronal physiology; synaptic plasticity

*Corresponding author. Institute of Genetics, Rheinische Friedrich-Wilhelms University, Molecular Genetics of Cell Migration, Römerstrasse 164, Bonn 53117, Germany.
Tel.: +49 228 73 4211; Fax: +49 228 73 4263;
E-mail: w.witke@uni-bonn.de

**Received: 26 August 2009; accepted: 26 March 2010; published online: 20 April 2010**

## Introduction

A fundamental property of synapses is their ability to modulate the strength of connectivity through various forms of synaptic plasticity. The different cellular processes contributing to synaptic plasticity are still not fully understood. Among the different models to describe synaptic plasticity, there has been growing interest in the dynamic remodelling of synapse structure. In particular, dendritic spines were shown to undergo dynamic shape changes that are driven by the actin cytoskeleton (Matus, 2000; Sorra and Harris, 2000). Apart from determining spine morphology, the actin cytoskeleton also has a more direct function in synaptic transmission (Dillon and Goda, 2005; Pilo Boyl *et al*, 2007; Cingolani and Goda, 2008) and the consolidation of long-term potentiation (LTP) (Fukazawa *et al*, 2003). These concepts have been well established in cultured neurons and brain slices; however, the *in vivo* relevance of actin dynamics for synaptic plasticity, learning and memory has largely remained elusive because of the lack of the respective animal models.

We have shown earlier that actin filament (F-actin) disassembly by n-cofilin is essential for cell shape and migration of neurons (Bellenchi *et al*, 2007), and results in knockout mice for LIM kinase1 (LIMK-1), a negative regulator of cofilin/*actin depolymerizing factor* (ADF), have suggested a potential function of n-cofilin in dendritic spine morphology (Meng *et al*, 2002). LIMK-1 and de-regulation of the cofilin pathway have been linked to Williams' syndrome, a particular form of mental retardation and autism spectrum disorder (Frangiskakis *et al*, 1996).

To directly approach the function of the cofilin pathway in synaptic plasticity, we designed a mouse model in which n-cofilin was selectively deleted from the principal neurons of the postnatal forebrain by using a conditional n-cofilin allele (n-cof$^{flx/flx}$) (Bellenchi *et al*, 2007) and a CamKII-cre line (Minichiello *et al*, 1999). This allowed us to uncouple the contribution of n-cofilin to early CNS development and to specifically address the function in postnatal synaptic physiology. Here, we show that n-cofilin is an important regulator of synaptic F-actin turnover and that loss of n-cofilin leads to accumulation of synaptic F-actin content. The accompanied changes in the actin cytoskeleton lead to increased synapse density in the hippocampus and enlargement of dendritic spines. In addition, we reveal a novel n-cofilin and actin-dependent mechanism of AMPA receptor (AMPAR) mobility and confinement. Consistent with a specific function of n-cofilin in synaptic plasticity, we observed severe impairment of associative learning in n-cofilin mutant mice, whereas exploratory or latent learning seemed to be unaffected. In conclusion, n-cofilin-dependent actin dynamics is not essential for general neuronal morphology and function, but specifically controls dendritic spine shape and AMPAR availability as well as synaptic plasticity during associative learning.

## Results

### *Synaptic localization and function of n-cofilin*

The actin depolymerizing protein n-cofilin is broadly expressed in the mammalian brain (Meberg *et al*, 1998; Bellenchi *et al*, 2007). More specifically, we found n-cofilin in isolated cortical synaptosomes (Figure 1A), which is in agreement with earlier electron microscopic studies (Racz and Weinberg, 2006). The localization suggests a functional role of n-cofilin in regulating synaptic F-actin turnover. Similarly, also ADF, a close homologue of n-cofilin was present in synaptosomes. Fractionation of synaptosomal compartments revealed that both, n-cofilin and ADF, were mainly present in the soluble fraction, with low abundance in the presynaptic matrix and the postsynaptic density (PSD).

To reveal n-cofilin function at the synapse, we investigated n-cof$^{flx/flx,CaMKII\text{-}cre}$ mice in which n-cofilin was selectively removed from principal neurons of the postnatal forebrain. In n-cof$^{flx/flx,CaMKII\text{-}cre}$ mice, mRNA and protein levels were strongly reduced in the forebrain as determined by *in situ* hybridization experiments (Figure 1B) and immunoblots (Figure 1C–E), respectively. In lysates from hippocampus, cortex and cerebellum, the progression of n-cofilin deletion and protein loss can be monitored at postnatal day 1 (P1), P21 and P50. As expected, at P1, deletion was not detectable in n-cof$^{flx/flx,CaMKII\text{-}cre}$ mice, whereas at P50, the n-cofilin levels in hippocampus and cortex were reduced by $>90\%$ (Figure 1C and D). No loss of n-cofilin was observed in the cerebellum of n-cof$^{flx/flx,CaMKII\text{-}cre}$ mice, in which CaMKII-cre is not expressed (Figure 1E). Interestingly, compensatory overexpression of ADF was evident in hippocampus and cortex at P50. When brain lysates were enriched for the neuronal cell contribution by isolating synaptosomes from n-cof$^{flx/flx,CaMKII\text{-}cre}$ mice, n-cofilin was practically not detectable (Figure 1F), showing that the residual amounts of n-cofilin expression in n-cof$^{flx/flx,CaMKII\text{-}cre}$ hippocampus and cortex lysates are due to glia cell contribution rather than incomplete deletion. Again, compensatory up-regulation of ADF was seen in synaptosomes from n-cofilin mutant mice.

Cofilin/ADF activity can be regulated by phosphorylation. Phosphorylation of cofilin/ADF leads to inactivation and loss of actin binding (Bamburg and Wiggan, 2002). To investigate the relative amount of inactivated n-cofilin in n-cof$^{flx/flx,CaMKII\text{-}cre}$ mice, we used an antibody that specifically recognizes phospho-cofilin/ADF without differentiating between n-cofilin and ADF. To our surprise, phospho-cofilin/ADF was prominent at P1 and dramatically declined at later stages P21 and P50 (Figure 1D). Clearly, the phosphorylation pattern was uncoupled from the amount of n-cofilin in the cortex and one plausible explanation could be that ADF is the major phosphorylated form *in vivo*. A similar pattern was seen in hippocampus and cerebellum, although their overall phosphorylation levels were much weaker (data not shown).

To validate the premise that n-cofilin is regulating synaptic F-actin turnover, we determined the ratio of filamentous to monomeric actin (F/G-actin) in the synaptic compartment of n-cof$^{flx/flx,CaMKII\text{-}cre}$ mice. In isolated cortical and hippocampal synaptosomes, a 50–60% increase in the F/G-actin ratio was observed (Figure 1G). A similar increase in F-actin was seen in total brain lysates from different areas in which n-cofilin was deleted, whereas in cerebellum, as an internal control, the F-actin levels were not changed (Figure 1H). These results show that n-cofilin is critical to maintain the equilibrium of synaptic F-actin and G-actin.

### *Synapse density and dendritic spine morphology depend on n-cofilin*

F-actin dynamics is thought to contribute to dendritic spine morphology and synaptic plasticity (Tada and Sheng, 2006; Cingolani and Goda, 2008), and we reasoned that the increase in synaptic F-actin should give us the unique opportunity to correlate physiological changes in actin dynamics with dendritic spine morphology. To visualize dendritic spines *in vivo*, we, therefore, crossed the n-cof$^{flx/flx,CaMKII\text{-}cre}$ mice to the *Thy1*-green fluorescent protein (GFP)-M line (Feng *et al*, 2000). *Thy1*-GFP-M transgenic mice show mosaic expression of GFP in various brain regions. As GFP serves as a volume indicator, we used this tool to analyse the morphology of pyramidal neurons in the hippocampal CA1 region and their dendritic arborization in *stratum radiatum*. Interestingly, n-cofilin deletion had no adverse effects on the overall morphology and the dendritic branching of hippocampal pyramidal cells (Figure 2A and B), suggesting that brain development was not affected. However, when we imaged second-order dendritic branches in the CA1 *stratum radiatum* with high-resolution confocal microscopy (see Figure 2A and B for representative images), we found that the number and morphology of dendritic spines were dependent on n-cofilin. The density of dendritic spines in CA1 pyramidal neurons of n-cof$^{flx/flx,CaMKII\text{-}cre,Thy1\text{-}GFP}$ mice was significantly increased when compared with n-cof$^{flx/flx,Thy1\text{-}GFP}$ controls (Figure 2C). Specifically the number of mushroom-shaped spines was higher in mutant mice, whereas the number of filopodia-like spines was not significantly changed. In addition, dendritic spine heads were larger in n-cof$^{flx/flx,CaMKII\text{-}cre,Thy1\text{-}GFP}$ mice as shown by the area distribution curve (Figure 2D) and the corresponding mean values (inset). A tendency for increased head/neck ratio was observed in mutants (Figure 2E). Although this increase was not statistically significant, a subpopulation of 15–20% of mutant spines showed a substantial enlargement of head area relative to the neck length (arrows). This result was confirmed in long-term cultured GFP-transfected hippocampal neurons from n-cof$^{flx/flx,CaMKII\text{-}cre}$ mice. Analysis of spine length and width (see Figure 2G for representative images) also showed an increase in dendritic spine size on deletion of n-cofilin (Figure 2H). It is important to note that deletion efficiency of n-cofilin in cultured hippocampal neurons was similar to what we observed in hippocampal brain lysates at P50 (Figure 2F).

The alterations in dendritic spine morphology were further confirmed by electron microscopy. In n-cof$^{flx/flx,CaMKII\text{-}cre}$ mice (see Figure 3A for representative images), a 40% increase in the density of axo-spinous synapses in the *stratum radiatum* was seen (Figure 3B). Moreover, morphometric analysis of the synapse ultrastructure confirmed the significant increase of the spine head area (Figure 3C) that was paralleled by an increase in the PSD length (Figure 3D). Interestingly, the area of the presynaptic boutons (Figure 3E) and the length of the active zone (Figure 3F) were also enlarged.

Together, these results show that deleting n-cofilin and blocking of F-actin disassembly will increase neuronal connectivity and favour spine swelling *in vivo*. These data

 

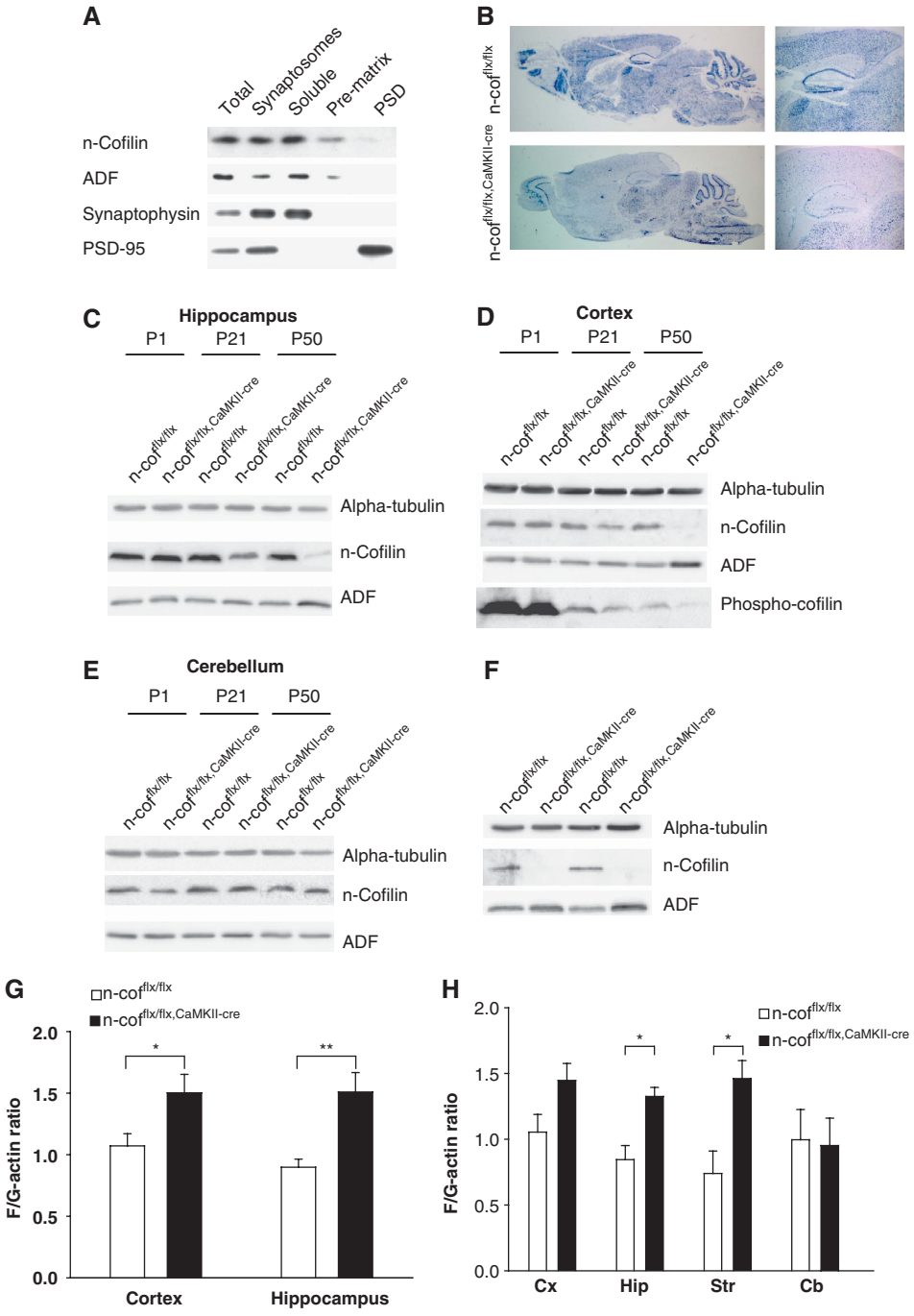


**Figure 1** Synaptic localization, forebrain-specific deletion of n-cofilin and synaptic F-actin content. (**A**) The n-cofilin and ADF were present in cortical synaptosomes. Both proteins were predominantly located in the synaptophysin-positive soluble fraction and the presynaptic matrix fraction (Pre-matrix). (**B**) Forebrain-specific deletion of n-cofilin was confirmed by *in situ* hybridization in 12-week-old mice. Region of the hippocampus is shown magnified. (**C**) Protein lysates of hippocampal preparations from n-cof$^{flx/flx,CaMKII\text{-}cre}$ mice revealed no changes in n-cofilin expression levels at P1 and a strong reduction at P21. In early adulthood (P50), n-cofilin expression was reduced to 8.60 ± 2.33% ($n = 3$). At P50, ADF levels were increased to 165.59 ± 17.23% ($n = 3$) in mutant hippocampus when compared with controls. (**D**) Likewise, n-cofilin expression in n-cof$^{flx/flx,CaMKII\text{-}cre}$ cortex was not affected at P1 and strongly reduced at P21. At P50, n-cofilin expression in n-cof$^{flx/flx,CaMKII\text{-}cre}$ mice was 6.66 ± 2.02% of control level ($n = 3$). As in the hippocampus, ADF was up-regulated in the cortex of n-cof$^{flx/flx,CaMKII\text{-}cre}$ mice (179.67 ± 24.63%; $n = 3$). Immunoblot analysis further revealed that in the cortex of n-cof$^{flx/flx,CaMKII\text{-}cre}$ mice and controls, the phospho-cofilin signal was high at P1 and decreased at P21 in both groups. Compared with controls, the amount of phospho-cofilin was reduced in mutant mice at P21 and P50. (**E**) Immunoblot analysis of protein lysates from cerebellum of n-cof$^{flx/flx,CaMKII\text{-}cre}$ mice showed no changes in n-cofilin and served as an internal control. (**F**) In synaptosomal preparations from hippocampal tissue of 12-week-old mice n-cofilin was practically absent in n-cof$^{flx/flx,CaMKII\text{-}cre}$ mice (2.01 ± 0.42%; $n = 4$), and ADF was increased (129.12 ± 4.7% ($n = 4$)). (**G**) F/G-actin ratios were increased in cortical (1.07 ± 0.09 versus 1.50 ± 0.15; $P < 0.05$; $n \geqslant 6$) and hippocampal synaptosomes (0.90 ± 0.07 versus 1.51 ± 0.14; $P < 0.01$; $n \geqslant 6$) of 12-week-old n-cof$^{flx/flx,CaMKII\text{-}cre}$ mice. (**H**) F/G-actin ratios were significantly increased in hippocampal (0.84 ± 0.11 versus 1.33 ± 0.07; $P < 0.05$; $n \geqslant 5$) and striatal lysates (0.74 ± 0.15 versus 1.46 ± 0.14; $P < 0.05$; $n \geqslant 5$) of 10-week-old n-cof$^{flx/flx,CaMKII\text{-}cre}$ mice, but not in cerebellar lysates used as an internal control. A tendency towards more F-actin was found in cortical lysates (1.05 ± 0.13 versus 1.45 ± 0.13; $P = 0.08$; $n \geqslant 5$). $^{*}P < 0.05$, $^{**}P < 0.01$.

underscore the important function of n-cofilin in synaptogenesis and in controlling dendritic spine morphology.

### *The n-cofilin-dependent hippocampal LTP and long-term depression*

The alteration in spine morphology and synaptic actin dynamics suggested that postnatal n-cofilin deletion could impact on synaptic plasticity. To test this hypothesis, we performed extracellular field potential recordings in acute slices of the hippocampal CA1 region. This analysis revealed that in the absence of n-cofilin, presynaptic functions in the Schaffer collateral-CA1 (Sc-CA1) pathway were fully preserved. The fEPSP slope elicited by fibre volleys did not differ between n-cof$^{flx/flx,CaMKII\text{-}cre}$ mice and controls (Figure 4A). Similarly, paired-pulse facilitation (Figure 4B), as well as post-tetanic potentiation (Figure 4C) and short-

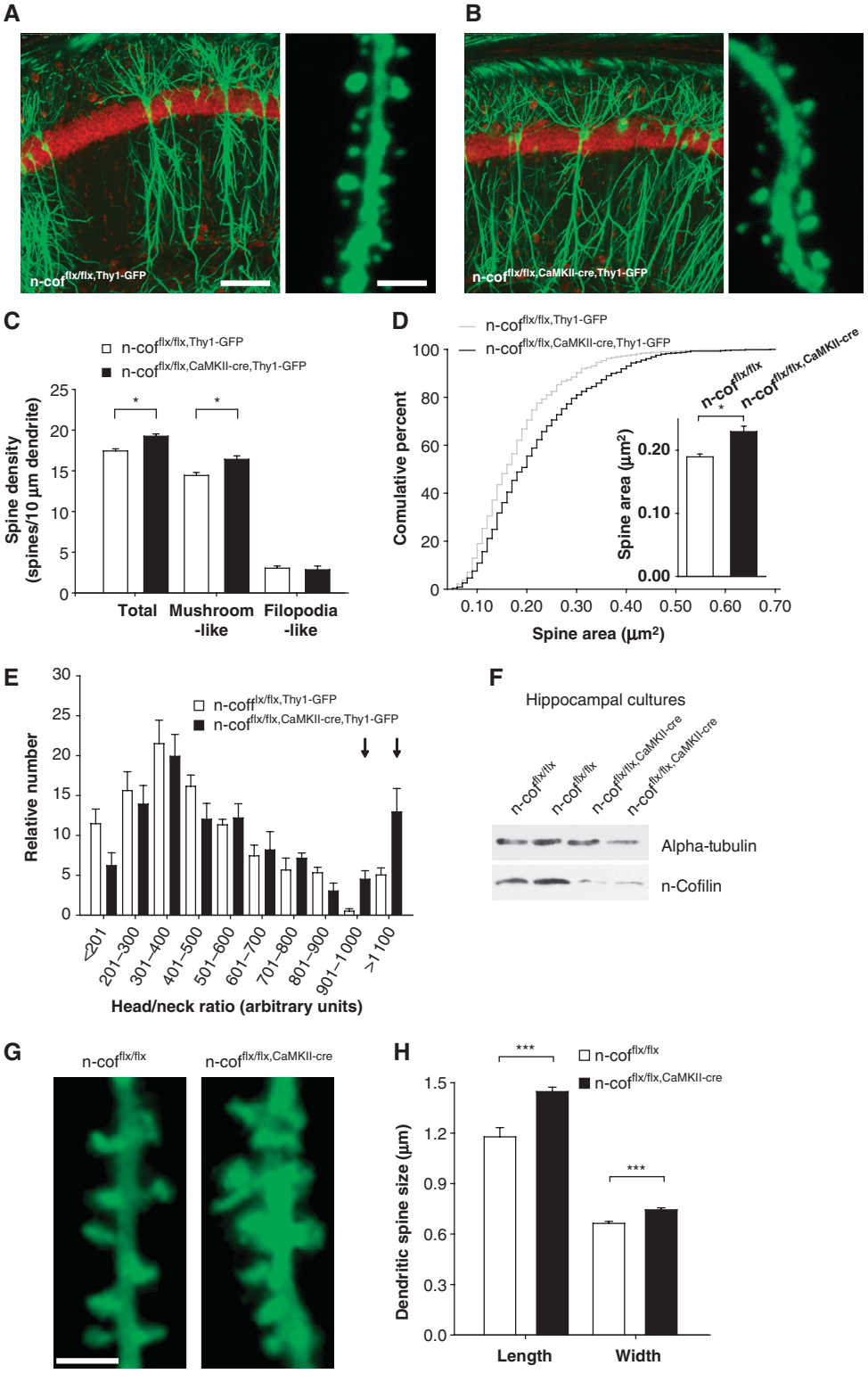

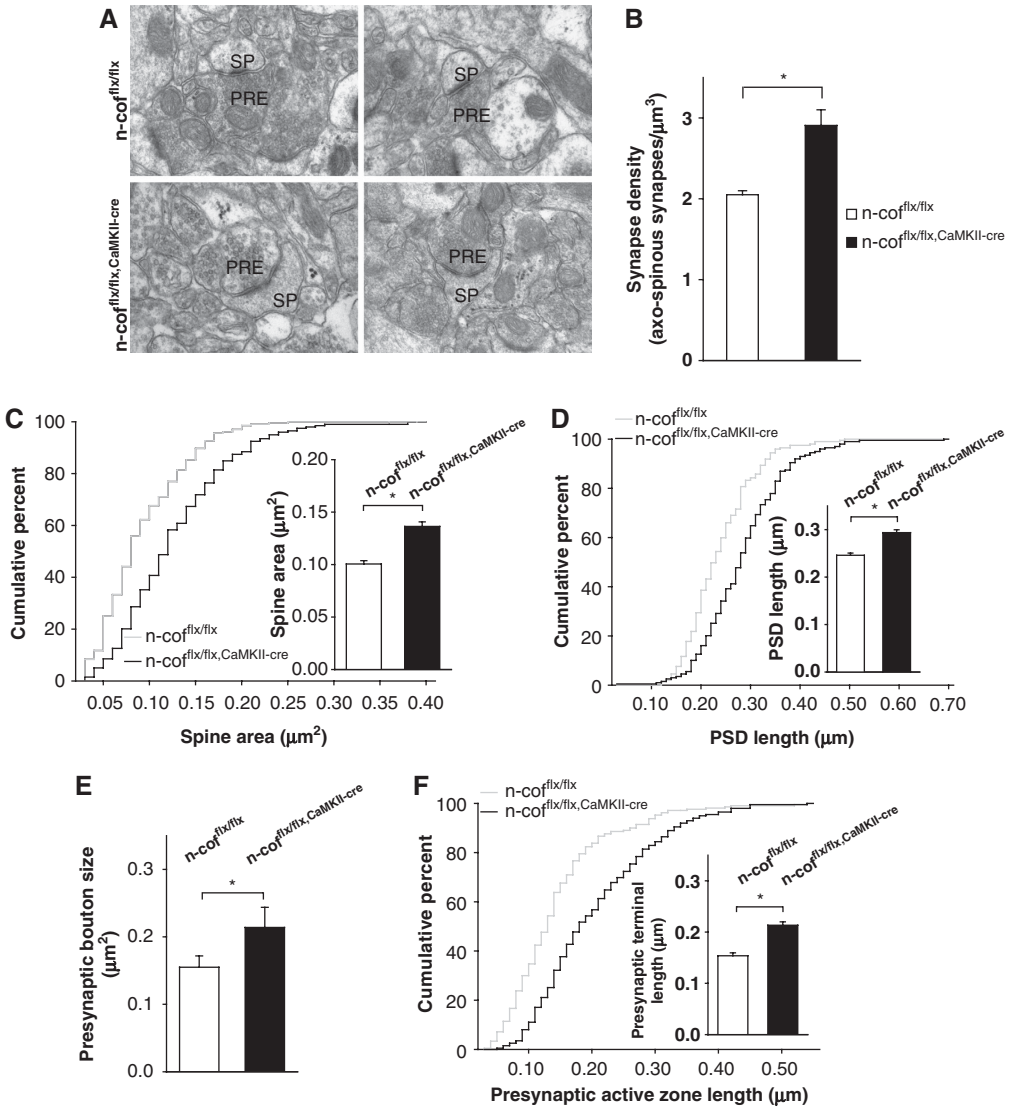


**Figure 3** Increased density and enlarged axo-spinous synapses. (**A**) Representative electron micrographs of CA1 *stratum radiatum* of 8-week-old n-cof$^{flx/flx,CaMKII\text{-}cre}$ mice and n-cof$^{flx/flx}$ controls (SP, spines; PRE, presynaptic terminal). (**B**) Density of axo-spinous synapses in CA1 *stratum radiatum* is elevated in n-cof$^{flx/flx,CaMKII\text{-}cre}$ mice ($2.06 \pm 0.03$ versus $2.91 \pm 0.19$ synapses/$\mu m^3$; $P<0.05$; $n=3$). (**C**) Cumulative percentage curves of dendritic spine area from CA1 hippocampal *stratum radiatum* (controls, $n=204/3$; n-cof$^{flx/flx,CaMKII\text{-}cre}$, $n=199/3$). Inset shows mean spine area values ($0.099 \pm 0.003$ versus $0.135 \pm 0.001$ $\mu m^2$; $P<0.01$). (**D**) Cumulative distribution PSD length ($n=197/3$ for control and 199/3 for n-cof$^{flx/flx,CaMKII\text{-}cre}$). Inset shows mean values of PSD length ($0.247 \pm 0.005$ versus $0.294 \pm 0.006$ μm; $P<0.01$). (**E**) Increase in presynaptic bouton size in n-cof$^{flx/flx,CaMKII\text{-}cre}$ mice ($0.155 \pm 0.017$ versus $0.214 \pm 0.030$ $\mu m^2$; $P<0.001$). (**F**) Length of the presynaptic active zone as shown by the cumulative distribution ($n=210/3$ for control and 199/3 for n-cof$^{flx/flx,CaMKII\text{-}cre}$). Inset shows the mean values ($0.154 \pm 0.006$ versus $0.213 \pm 0.007$ μm; $P<0.01$). $^*P<0.05$.

**Figure 2** Altered dendritic spine density and morphology. *Thy1*-GFP-M transgene was crossed into n-cof$^{flx/flx,CaMKII\text{-}cre}$ background to assess neuronal morphology and branching of CA1 hippocampal pyramidal cells in 8-week-old mice. Coronal sections of *Thy1*-GFP-M-expressing n-cof$^{flx/flx}$ controls (**A**) and n-cof$^{flx/flx,CaMKII\text{-}cre}$ mutants (**B**) showed no differences in overall neuron morphology. White calibration bar corresponds to 100 μm. High magnifications in (**A**) and (**B**) show representative images of second-order branches in the proximal region of the hippocampal CA1 *stratum radiatum*. Calibration bar corresponds to 4 μm. (**C**) Linear density of dendritic spines in the *stratum radiatum* ($17.44 \pm 0.25$ versus $19.25 \pm 0.28$ spines/10 μm dendrite; $P<0.05$; $n=3421$ dendritic spines/4 n-cof$^{flx/flx,Thy1\text{-}GFP}$ controls and 3325/4 for n-cof$^{flx/flx,CaMKII\text{-}cre,Thy1\text{-}GFP}$ mice) and of mushroom-like dendritic spines ($14.43 \pm 0.37$ versus $16.40 \pm 0.43$ spines/10 μm dendrite; $P<0.05$) were significantly increased in n-cof$^{flx/flx,CaMKII\text{-}cre,Thy1\text{-}GFP}$ pyramidal cells. Filopodia-like protrusions were not altered ($3.03 \pm 0.28$ versus $2.84 \pm 0.46$ spines/10 μm dendrite). (**D**) Enlargement of dendritic spines in n-cof$^{flx/flx,CaMKII\text{-}cre,Thy1\text{-}GFP}$ mice as shown by cumulative distribution of spine area and (inset) mean values ($0.19 \pm 0.01$ versus $0.23 \pm 0.01$ $\mu m^2$; $P<0.05$; $n=737$ spines/4 mice for n-cof$^{flx/flx,Thy1\text{-}GFP}$ and 696/4 for n-cof$^{flx/flx,CaMKII\text{-}cre,Thy1\text{-}GFP}$). (**E**) Distribution of head/neck ratios of dendritic spines of CA1 pyramidal cells. For each spine, head area and neck length were measured using stacks of confocal images ($n=359/4$ for n-cof$^{flx/flx,Thy1\text{-}GFP}$ and 342/4 for n-cof$^{flx/flx,CaMKII\text{-}cre,Thy1\text{-}GFP}$). (**F**) Immunoblot analysis of protein lysates obtained from DIV 21 primary hippocampal cultures revealed strong reduction of n-cofilin. (**G**) Representative images of dendritic spines from GFP-transfected hippocampal pyramidal cells in culture at DIV 21. Calibration bar corresponds to 2 μm. (**H**) Morphometric analyses showed spine enlargement in n-cof$^{flx/flx,CaMKII\text{-}cre}$ neurons as deduced from significant increases in spine length ($1.178 \pm 0.055$ versus $1.447 \pm 0.026$ μm; $P<0.0001$; $n=304$ spines for n-cof$^{flx/flx}$ controls and 439 for n-cof$^{flx/flx,CaMKII\text{-}cre}$ mice) and width ($0.663 \pm 0.012$ versus $0.744 \pm 0.012$ μm; $P<0.0001$). $^*P<0.05$, $^{***}P<0.001$.

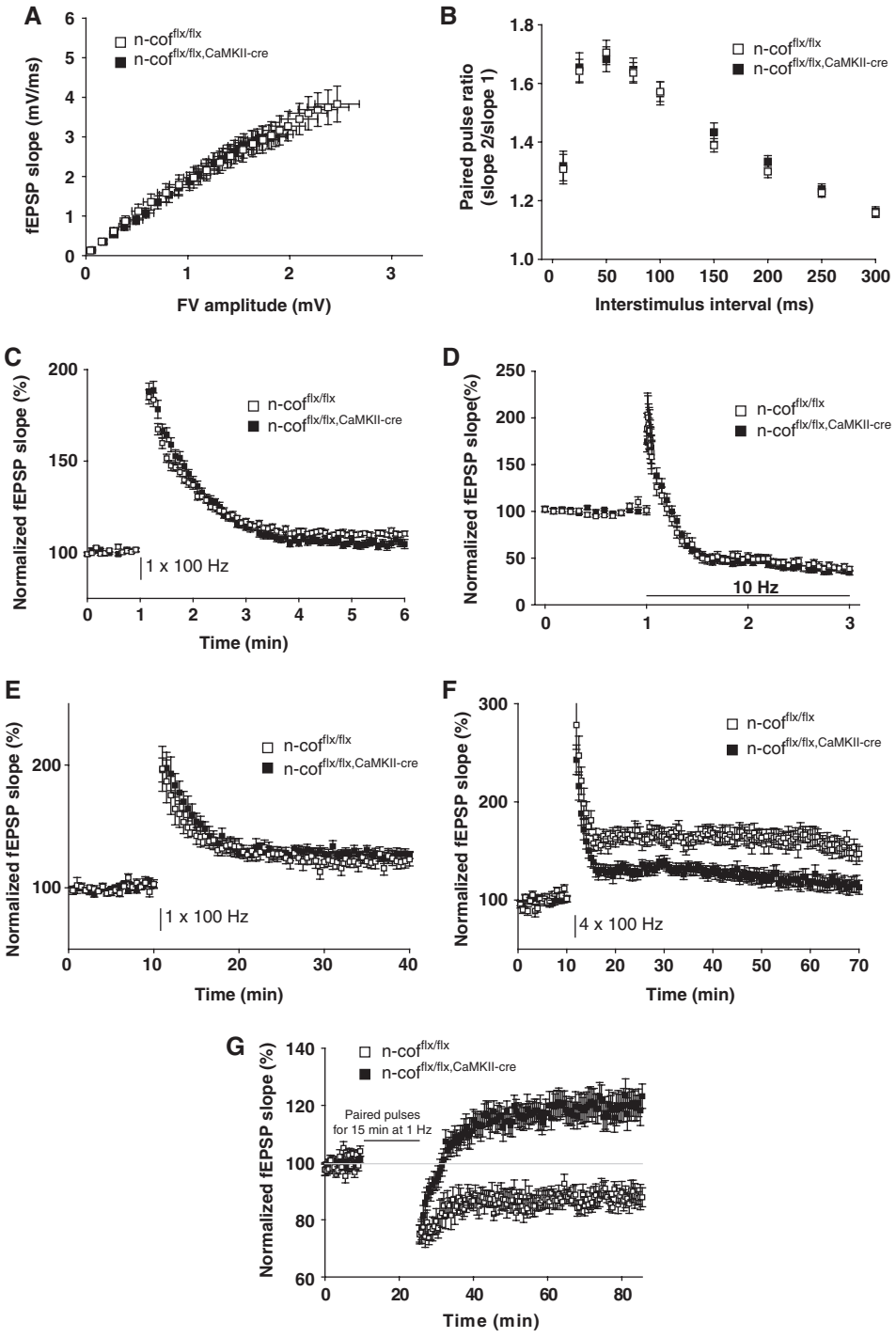


**Figure 4** Normal presynaptic function and E-LTP, but altered L-LTP and LTD. (**A**) Basal synaptic transmission is normal in Schaffer-collateral-CA1 synapses of n-cof$^{flx/flx,CaMKII\text{-}cre}$ mice ($n=29$ for n-cof$^{flx/flx}$ and 30 for n-cof$^{flx/flx,CaMKII\text{-}cre}$). (**B**) Paired-pulse facilitation is not altered ($n=18$ for both groups), (**C**) post-tetanic potentiation ($n=16$ for n-cof$^{flx/flx}$ and 17 for n-cof$^{flx/flx,CaMKII\text{-}cre}$) and (**D**) short-term depression ($n=19$ for both groups) indicates normal presynaptic function in n-cof$^{flx/flx,CaMKII\text{-}cre}$ mice. (**E**) E-LTP in Schaffer collateral-commissural CA1 synapses elicited by a single stimulation of 1 s with 100 Hz was comparable in n-cof$^{flx/flx,CaMKII\text{-}cre}$ mice and controls ($n=8$ for n-cof$^{flx/flx}$ and 10 for n-cof$^{flx/flx,CaMKII\text{-}cre}$). (**F**) When applying four trains of 1 s duration to induce L-LTP, potentiation was significantly decreased in n-cof$^{flx/flx,CaMKII\text{-}cre}$ mice compared with controls ($n=11$ for both groups). (**G**) Paired-pulse LFS induces LTD in control mice. In n-cof$^{flx/flx,CaMKII\text{-}cre}$ mice, a synaptic potentiation was seen ($n=9$ for n-cof$^{flx/flx}$ and 13 for n-cof$^{flx/flx,CaMKII\text{-}cre}$). Age of mice was between P14 and P24 for LTD and between P35 and P46 for all other electrophysiological recordings.

term depression in the presence of the NMDA receptor (NMDAR) antagonist APV (Figure 4D) were not significantly altered in n-cof$^{flx/flx,CaMKII\text{-}cre}$ mice. From these data we concluded that presynaptic parameters of synaptic transmission such as neurotransmitter release and presynaptic short-term plasticity were not affected on n-cofilin deletion.

We then performed a battery of experiments to address the function of n-cofilin in long-term plasticity. When LTP

 

was induced by a single 100 Hz tetanus of 1 s duration at Sc-CA1 synapses, no differences were observed between n-cof$^{flx/flx,CaMKII\text{-}cre}$ and control mice (Figure 4E). However, when we applied a protocol consisting of four 100 Hz tetani of 1 s duration, which is thought to evoke late-LTP (L-LTP) (Albensi *et al*, 2007; Reymann and Frey, 2007), potentiation was significantly reduced in n-cof$^{flx/flx,CaMKII\text{-}cre}$ mice (Figure 4F). After 60 min of tetanic stimulation, a potentiation of 150% was found in controls compared with 120% in mutant mice.

Interestingly, Sc-CA1 synapses in n-cof$^{flx/flx,CaMKII\text{-}cre}$ mice were found to be resistant to long-term depression (LTD). Whereas a robust depression of about 15% was inducible in controls by low 1 Hz frequency stimulation, n-cof$^{flx/flx,CaMKII\text{-}cre}$ mice responded with a potentiation of roughly 20% (Figure 4G).

Two important conclusions can be drawn from these results. First, n-cofilin-driven F-actin dynamics is important for postsynaptic mechanisms such as L-LTP or LTD, whereas it seems to be dispensable for all tested presynaptic activities. Second, the *in vivo* findings are in contrast to *in vitro* observations on isolated cultured neurons, in which pharmacological stabilization of F-actin was shown to affect both pre- and postsynaptic activities (Kim and Lisman, 1999).

### *AMPAR mobility requires n-cofilin activity*

To better understand the molecular mechanisms that contribute to the alterations of synaptic plasticity in n-cof$^{flx/flx,CaMKII\text{-}cre}$ mice, we first wanted to ensure that deletion of n-cofilin had no major effect on the composition of the PSD itself. Expression of AMPAR-associated proteins such as stargazin/TARP γ2, TARP γ8, NSF and GRIP/ABP, or important PSD proteins such as the membrane-associated guanylate kinases Chapsyn-110/PSD-93, spontaneous alternation performance 102 (SAP102) and PSD-95/SAP-90 or Shank1 was not affected by n-cofilin deletion (Figure 5A). Similarly, hippocampal NMDAR surface expression was not changed in n-cof$^{flx/flx,CaMKII\text{-}cre}$ mice as judged by receptor binding of *[$^3$H]-MK801* (Figure 5B). On the contrary, AMPAR surface expression was found to be slightly increased in rostral parts, but not in the caudal parts of the hippocampus (Figure 5C). However, using electrophysiology, we could show that the ratio between AMPAR- and NMDAR-mediated currents is not significantly altered in CA1 pyramidal cells of n-cof$^{flx/flx,CaMKII\text{-}cre}$ mice (Figure 5D). Taken together, these data indicate that the composition of the PSD is not affected on deletion of n-cofilin.

The slight alteration in AMPAR surface concentration possibly reflects local changes of AMPAR such as synaptic recruitment and clustering. In particular, the exchange of AMPAR between synaptic and extrasynaptic domains by lateral diffusion is thought to represent a novel mechanism, which allows to control synaptic AMPAR concentration during modulation of synaptic plasticity (Borgdorff and Choquet, 2002; Tardin *et al*, 2003).

To test whether n-cofilin-driven actin dynamics could influence synaptic exchange of AMPAR, we quantified the lateral diffusion of AMPAR directly by single particle tracking.

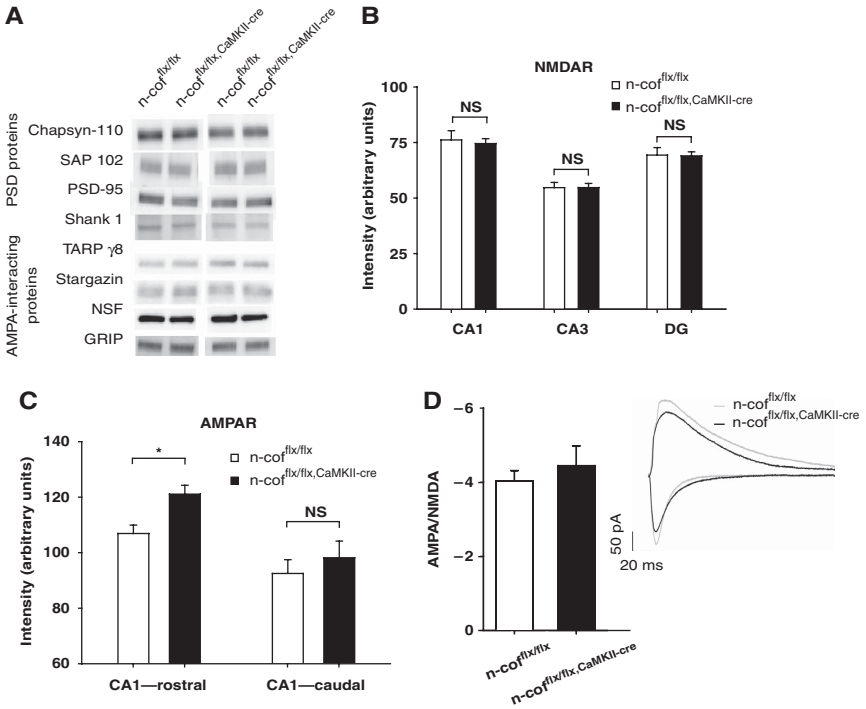


**Figure 5** Synaptic content and surface expression of NMDAR and AMPAR. (**A**) Expression of PSD proteins (Chapsyin-110/PSD-93, SAP102, PSD-95/SAP90, Shank1), as well as AMPAR-interacting proteins (stargazing/TARP γ2, TARP γ8, NSF, GRIP/ABP) were unchanged in synaptosomes of 12-week-old n-cof$^{flx/flx,CaMKII\text{-}cre}$ mice. (**B**) NMDAR surface expression, analysed by radio-ligand binding of [$^3$H]-labelled MK-801 was unchanged in the hippocampal regions examined (CA3, CA1, dentate gyrus, DG) ($n=24$ coronal section of four mice for each group). (**C**) Binding of [$^3$H]-labelled AMPA was increased in rostral parts ($106.92 \pm 3.03$ arbitrary units for controls versus $121.08 \pm 3.19$ arbitrary units n-cof$^{flx/flx,CaMKII\text{-}cre}$ mice; $P<0.05$; $n=24$ coronal section of four mice for each group), but not in caudal parts of the hippocampal CA1 region of n-cof$^{flx/flx,CaMKII\text{-}cre}$ mice. Age of mice used for ligand-binding assays was 12 weeks. (**D**) Bar graphs showing the average ratio of AMPAR- to NMDAR-mediated currents in control ($n=16$) and n-cof$^{flx/flx,CaMKII\text{-}cre}$ mice ($n=11$). Sample traces are shown on the right. Age of mice was between P35 and P46. $^*P<0.05$.

Antibodies against the extracellular domain of the GluR2-subunit were coupled to quantum dots (QDs) and the lateral diffusion of single AMPAR was tracked in cultured hippocampal neurons. In n-cof$^{flx/flx,CaMKII\text{-}cre}$ neurons, AMPAR diffusion was significantly slowed down in extrasynaptic domains, but not in synaptic regions (Figure 6A–C; Supplementary Table SI, movies S1 and S2). Also AMAPR confinement as deduced from their spatial exploration was reduced (Supplementary Table SII). In contrast, the diffusion and confinement of cholera toxin (ChTx), a marker for lipid rafts, was not affected by the lack of n-cofilin (Figure 6D and E; Supplementary Table SI and SII), suggesting that the effect is specific for receptors and not a general problem of membrane fluidity in n-cof$^{flx/flx,CaMKII\text{-}cre}$ neurons. To reinforce that n-cofilin function in AMPAR diffusion is likely through the actin cytoskeleton, we complemented the genetic experiments by pharmacological intervention with actin dynamics in hippocampal neurons. In our hands, latrunculin A, an inhibitor of actin polymerization, increased AMPAR mobility, whereas the F-actin stabilizing agent jasplakinolide reduced AMPAR mobility (Figure 6F and G; Supplementary Table SIII). These findings are consistent with our data on n-cofilin deletion and the increase in F-actin. One difference to the genetic n-cofilin model was that drugs affected both extrasynaptic and synaptic diffusion. The n-cofilin has a compartment-specific function, whereas actin drugs are not selective in disturbing the cellular actin pools.

### *Associative learning but not latent learning is impaired in n-cof$^{flx/flx,CaMKII\text{-}cre}$ mutant mice*

Our data show that n-cofilin controls dendritic spine morphology, synaptogenesis as well as AMPAR availability in the synapse. The n-cof$^{flx/flx,CaMKII\text{-}cre}$ mutants, therefore, provide a valuable genetic model, in which a potential link of actin dynamics and receptor diffusion and its relevance for learning and memory can be addressed (Choquet and Triller, 2003; Triller and Choquet, 2005). We used different paradigms of associative learning, including spatial learning, aversive learning and rewarded learning. The Morris water maze (MWM) paradigm addresses hippocampal-dependent spatial learning and memory (D'Hooge and De Deyn, 2001). In this test, n-cof$^{flx/flx,CaMKII\text{-}cre}$ mice were not able to learn the position of a hidden platform as indicated by increased tracking paths to reach the platform (Figure 7A). Consequently, mutant mice performed significantly weaker in the probe trial. When the platform was removed, n-cof$^{flx/flx,CaMKII\text{-}cre}$ mice were lacking a clear preference for the target quadrant (Figure 7B). The learning deficits of n-cof$^{flx/flx,CaMKII\text{-}cre}$ mice were best presented by plotting the distribution of individual mouse performance against the single learning sessions. Controls clustered around low latency values already after the first day of training and showed clear progress when trials 1 and 4 of each session performed at 20 min intervals were compared (Figure 7C). In contrast, the mutants' performance remained scattered with stochastic distribution throughout the entire 5-day training period and mice did not show improvement within individual sessions (Figure 7D). To exclude secondary problems because of visual perception or swimming performance, we tested n-cof$^{flx/flx,CaMKII\text{-}cre}$ mice also with a visible platform. In both tests, mutant mice performed similar to control mice (Figure 7E and F).

For aversive learning, we chose the classical fear conditioning (CFC) that involves both the hippocampus and the amygdala. In CFC, n-cof$^{flx/flx,CaMKII\text{-}cre}$ mice were strongly impaired in associating an aversive experience (foot shock) with different cues (a tone or chamber context). When testing contextual memory (24 h after training) and cued memory (36 h after training), mutant mice showed significantly lower freezing rates (Figure 7G). These deficits could be either because of impaired learning or memory consolidation. To further address this question, we challenged another cohort of animals by testing them immediately after the training session. Again, mutant mice showed less freezing when exposed to context and cue (Figure 7H), suggesting learning deficits as the main problem.

Both the MWM and the CFC provide strong stimuli to induce learning. An important question is whether the absence of n-cofilin would affect only those circuits relevant for aversive learning, or whether the mutation had a broad general impact on synaptic plasticity. To address this issue, we performed the 'conditioned place preference' paradigm using cocaine to associate a positive stimulus with a certain place. However, also in this reward-based learning task, n-cof$^{flx/flx,CaMKII\text{-}cre}$ mice performed poorly compared with controls (Figure 8A), suggesting that synaptic plasticity is generally impaired in all circuits required for associative learning.

Learning and memory are intimately linked and difficult to dissect experimentally. Lack of n-cofilin seems to mainly impair the active learning process, and we, therefore, decided to take advantage of a free exploration paradigm that would not involve any strong stimulus and would also allow us to test for short-term working memory deficits (Gruart *et al*, 2006). We scored SAP in a Y-maze, which is widely used to assess working memory. Interestingly, no impairment was observed in n-cof$^{flx/flx,CaMKII\text{-}cre}$ mice in their ability to discriminate novel versus already visited arms. The total number of visited arms (not shown), the SAP as well as the relative number of alternate arm returns or same arm returns were not different in mutant mice (Figure 8B). A similar result was obtained in the hole-board test, another free exploration paradigm that is believed to rely on working memory. Again, n-cof$^{flx/flx,CaMKII\text{-}cre}$ mice were indistinguishable from controls (Figure 8C). To further strengthen the finding that working memory is functioning in n-cof$^{flx/flx,CaMKII\text{-}cre}$ mice, we performed a third task, in which mice have to discriminate between a non-baited, earlier visited arm and a baited, earlier not visited arm of the Y-maze. In addition, in this test, the performance of n-cof$^{flx/flx,CaMKII\text{-}cre}$ mice was comparable with that of n-cof$^{flx/flx}$ controls (Figure 8D).

In summary, we can conclude that n-cofilin-dependent actin dynamics is specifically required for associative learning, whereas short-term working memory and exploratory learning is n-cofilin independent.

## Discussion

Actin is the most abundant cytoskeletal protein found at synapses; however, our understanding of the specific functions in pre- and postsynaptic physiology is still limited. In neuronal cultures and brain slices, actin has been implicated in the organization of the presynaptic vesicle pool, the

 

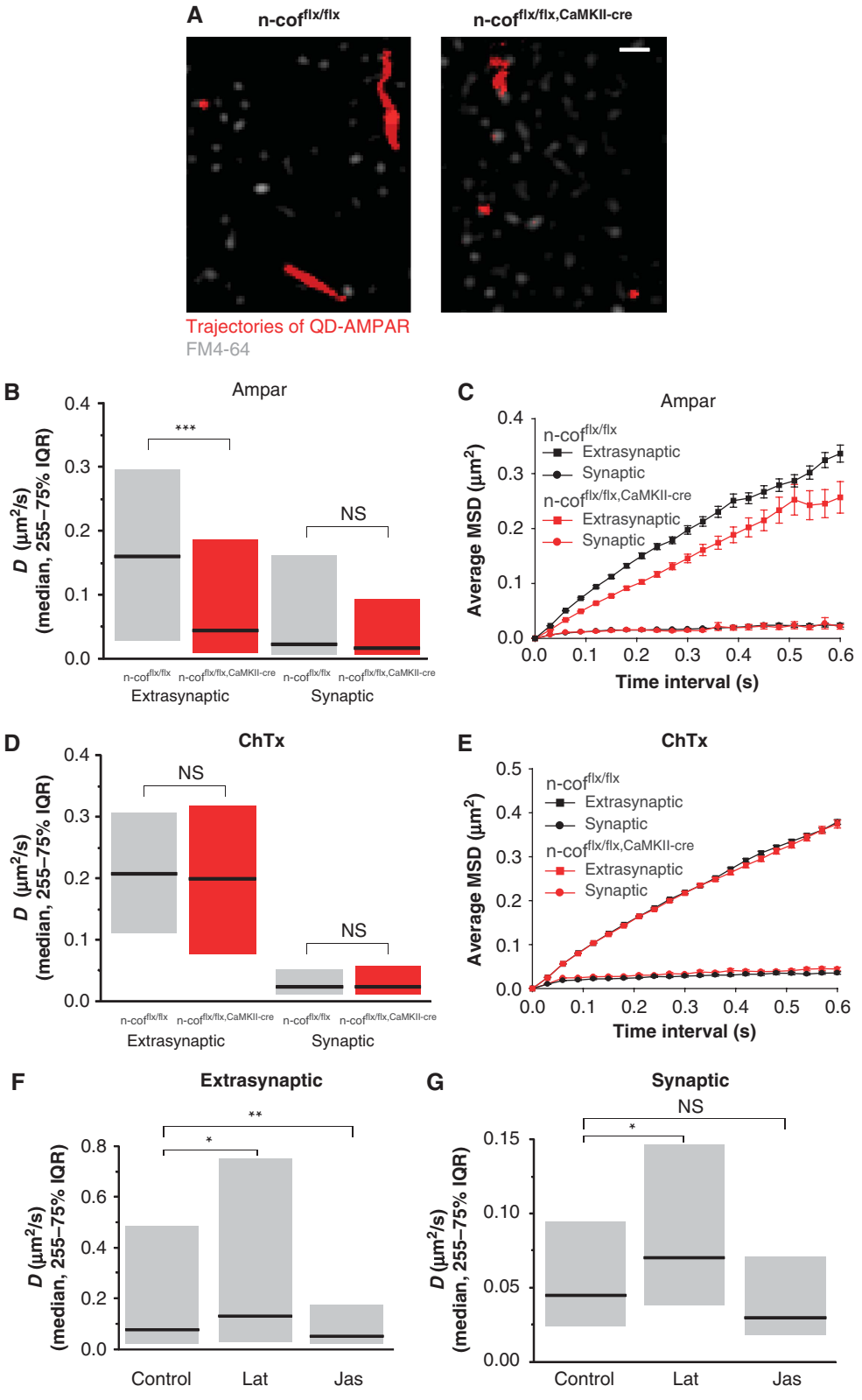


**Figure 6** Actin-dependent diffusion of AMPAR. (**A**) Trajectories of QD-bound AMPAR (red) in hippocampal neurons of n-cof$^{flx/flx}$ controls and n-cof$^{flx/flx,CaMKII\text{-}cre}$ mice (left and right panel, respectively). Synapses were identified by FM4-64 labelling (grey). Scale bar: 2 μm. (**B**) Distribution of the diffusion coefficient D for QD-AMPAR trajectories in n-cof$^{flx/flx}$ (grey) and n-cof$^{flx/flx,CaMKII\text{-}cre}$ mice (red) with extrasynaptic or synaptic localization (median and 25–75% IQR; Mann–Whitney (MW) test, ns: not significant, $***P<0.001$). (**C**) Average mean square displacement (MSD) over time in n-cof$^{flx/flx}$ (black) and n-cof$^{flx/flx,CaMKII\text{-}cre}$ mice (red) with extrasynaptic (squares) or synaptic localization (circles). (**D**) Distribution of the diffusion coefficient D for QD-ChTx trajectories in n-cof$^{flx/flx}$ (grey) and n-cof$^{flx/flx,CaMKII\text{-}cre}$ mice (red) with extrasynaptic or synaptic localization (median and 25–75% IQR; MW test). (**E**) Average MSD over time in n-cof$^{flx/flx}$ (black) and n-cof$^{flx/flx,CaMKII\text{-}cre}$ mice (red) with extrasynaptic (squares) or synaptic localization (circles). (**F**) Distribution of the diffusion coefficient D for extrasynaptic Cy5-AMPAR trajectories in neurons treated with buffer solution (control), and after destabilizing F-actin with latrunculin A (lat) or after stabilizing F-actin with jasplakinolide (jas) (median and 25–75% IQR; MW test, $**P<0.01$). (**G**) Same as (**F**), but for the synaptic diffusion trajectories (median and 25–75% IQR; MW test, $*P<0.05$).

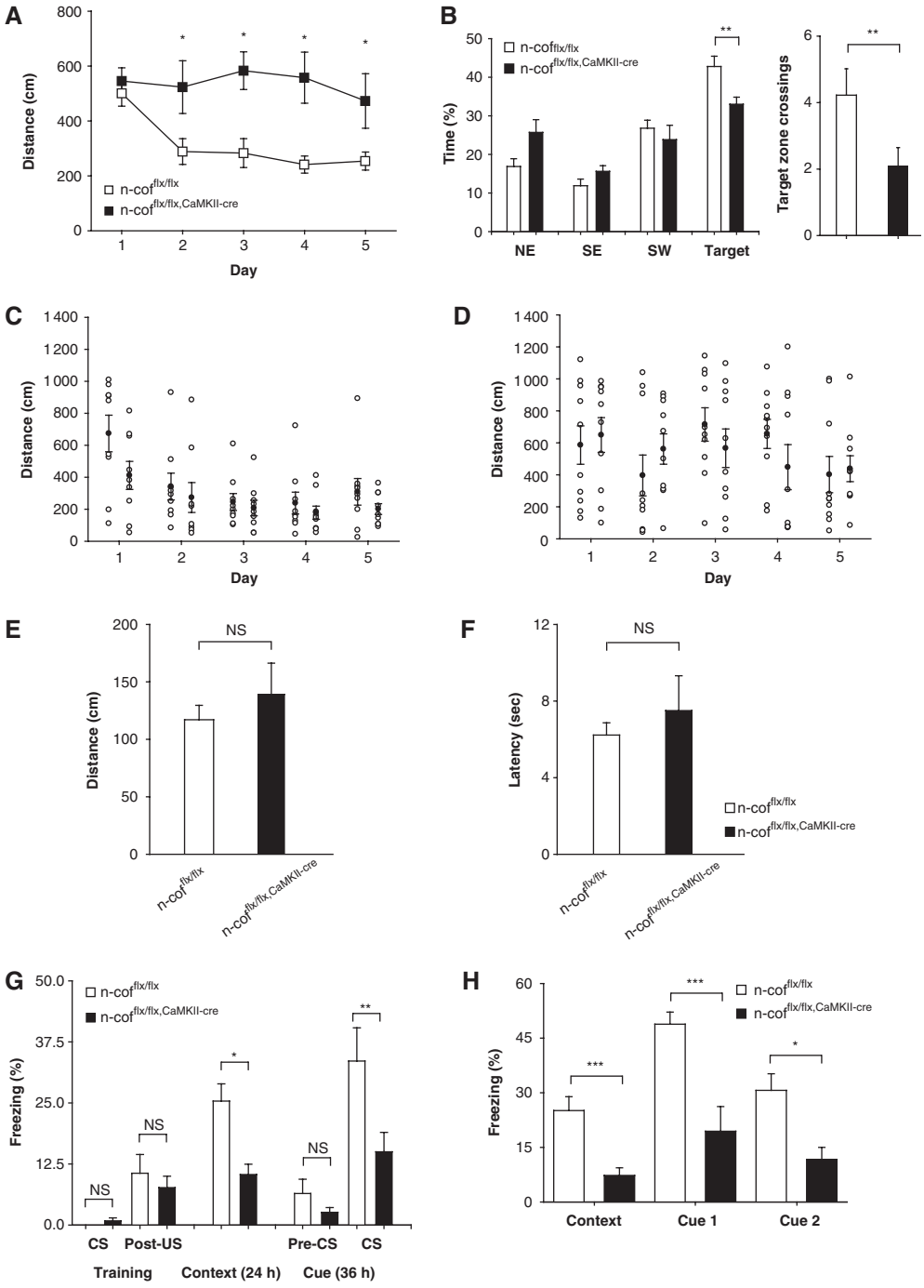


**Figure 7** Impaired associative learning in n-cof$^{flx/flx,CaMKII\text{-}cre}$ mice. (**A**) Impaired performance of n-cof$^{flx/flx,CaMKII\text{-}cre}$ mice during the 5 days testing period in the MWM as deduced from the distances before reaching the platform. (**B**) In the probe trial at day 6, n-cof$^{flx/flx,CaMKII\text{-}cre}$ mice spent significantly less time in the target quadrant ($P<0.05$) (left graph) and crossed less frequently the target zone ($P<0.01$) (right graph). (**C**) Individual performance of controls (open circles) ($n=9$) during the training period shows the improvement within a session by comparing trial 1 to trial 4 (inter trial interval: 20 min; closed circle represent mean distances). (**D**) Same analysis for n-cof$^{flx/flx,CaMKII\text{-}cre}$ mice ($n=10$) show no improvement even after 5 days of training. (**E**) In visible-flagged platform testing, n-cof$^{flx/flx,CaMKII\text{-}cre}$ mice performed similar to controls indicating that visual cues were perceived by mutants (NS: not significant different in Student's *t*-test). (**F**) Same experiment as in (**E**), but the latency of reaching the platform is shown. (**G**) During training of contextual fear conditioning (CFC) n-cof$^{flx/flx,CaMKII\text{-}cre}$ mice showed comparable freezing rates during a 30 s sound cue (CS) followed by a painful foot shock, excluding potential sensory problems. In the test experiment, 24 h later, n-cof$^{flx/flx,CaMKII\text{-}cre}$ mice ($n=14$) showed significantly less freezing compared with controls ($n=13$) when exposed to the aversive context ($P<0.05$). After 36 h of the training session, freezing was tested after exposure to the specific cue (sound). Again, freezing rates of n-cof$^{flx/flx,CaMKII\text{-}cre}$ mice were significantly decreased. (**H**) The entire CFC experiment (training, context and two series of cue testing, cue1 and cue2) was performed within 30 min to avoid long-term memory effects. In addition, in this paradigm, n-cof$^{flx/flx,CaMKII\text{-}cre}$ mice ($n=7$) did not learn to associate the context ($P<0.005$) and sound with the foot shock (cue1: $P<0.005$; cue2: $P<0.05$). Error bars indicate standard error of the mean. Age of mice used of behavioural experiments was between 10 and 16 weeks. $^{*}P<0.05$, $^{**}P<0.01$, $^{***}P<0.001$.

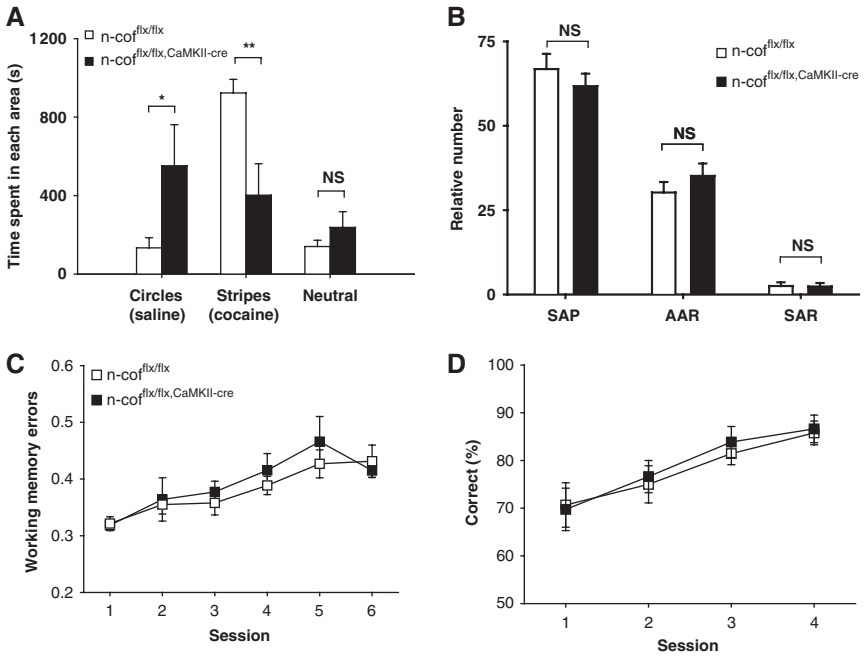


**Figure 8** Impaired reward induced learning and normal working memory in n-cof$^{flx/flx,CaMKII\text{-}cre}$ mice. (**A**) In the conditioned place, preference paradigm n-cof$^{flx/flx,CaMKII\text{-}cre}$ mice showed no preference for the reward-associated compartment '*stripes*'. Compared with controls, the mutant mice spent less time in the '*stripes*' compartment (923.0 ± 69.5 versus 402.1 ± 160.2 s; $P<0.01$; $n=7$ for n-cof$^{flx/flx}$ controls; $n=4$ for n-cof$^{flx/flx,CaMKII\text{-}cre}$ mice), and more time in the saline-associated compartment *circles* (133.6 ± 51.7 versus 552.1 ± 209.2 s; $P<0.05$). (**B**) In the Y-maze experiment, no significant differences were observed in the relative number of spontaneous alternation performance (SAP), alternate arm returns (AAR) or same arm returns (SAR) between n-cof$^{flx/flx,CaMKII\text{-}cre}$ mice and controls ($n=13$ for both groups). (**C**) In hole-board testing, working memory errors were not different in n-cof$^{flx/flx,CaMKII\text{-}cre}$ mice and control mice during all six sessions ($n=8$ for both groups). (**D**) In addition, no differences between n-cof$^{flx/flx,CaMKII\text{-}cre}$ mice ($n=14$) and controls ($n=16$) were found during a spatial working memory task using a modified Y-maze in which mice have to choose between a non-baited, earlier visited arm (incorrect response) and a baited arm, that was not visited before (correct response). Error bars indicate standard error of the mean. Age of mice used of behavioural experiments was between 10 and 16 weeks. $^*P<0.05$, $^{**}P<0.01$.

regulation of neurotransmitter release and the dynamic changes of dendritic spine morphology (Dillon and Goda, 2005; Cingolani and Goda, 2008). These functions are mainly based on pharmacological interference with actin polymerization and illustrates the essential function of synaptic actin; however, they also leave us with the dilemma to explain how specificity is introduced to the system. Actin itself is not sufficient for coordination and fine-tuning of the various neuronal processes, and actin-binding proteins that modulate the dynamic turnover of actin filaments in the synaptic compartments have, therefore, moved to the centre of attention. In addition, the *in vivo* relevance of these findings remains to be verified in genetic models for a comprehensive understanding of actin function.

Here, we have made an effort to address both questions—specificity and *in vivo* relevance of synaptic actin dynamics by examining n-cofilin as a modulator of neuronal physiology and animal behaviour.

Members of the cofilin/ADF family of F-actin depolymerizing proteins can accelerate filament turnover by generating new free filament ends and by enhancing the dissociation of actin subunits from the filament minus end (Bamburg and Wiggan, 2002). The n-cofilin is expressed in brain, and in neurons, the protein localizes predominantly to the dendritic spine periphery (Racz and Weinberg, 2006). On deletion of n-cofilin, the synaptic F-actin content is increased, showing the critical function of n-cofilin in controlling synaptic F-actin turnover. Hence, our conditional n-cof$^{flx/flx,CaMKII\text{-}cre}$ line provides a valuable model to address actin dynamics in synaptic transmission as well as the underlying molecular mechanisms. Apart from n-cofilin, ADF is the second cofilin/ADF family member expressed in brain. Gene deletion experiments have shown that n-cofilin, but not ADF, is essential during neuronal development (Bellenchi *et al*, 2007). Although both can be regulated by phosphorylation on Ser3, which inhibits F-actin depolymerization activity, it is not clear what significance cofilin/ADF phosphorylation has in brain physiology and synaptogenesis. Here, we discovered that phosphorylation levels are higher at early postnatal stages and dramatically decrease during the synaptogenesis period (P21–P50). The available antibodies do not distinguish between ADF and n-cofilin phosphorylation, and at this juncture, it is not clear which one accounts for the observed changes in phosphorylation. As cofilin/ADF phosphorylation is almost completely abolished at later postnatal stages, also in the n-cofilin mutant mice, one can assume that all ADF, which is still expressed, should be in the active form (see Figure 1C, D and F). However, this does not compensate for the loss of n-cofilin, highlighting the specificity of both proteins in neuronal function.

Another important conclusion from our studies is that n-cofilin is not essential for any of the tested presynaptic responses, but rather has a function for postsynaptic physiology. Dendritic spine morphology and synaptic connectivity are parameters, which are controlled by n-cofilin as shown by the increased spine size and higher number of synapses on deletion of n-cofilin. Normally, the F-actin pool in the spine periphery is highly dynamic (Halpain, 2000; Honkura *et al*,

2008), and actin remodelling in this region is thought to be responsible for the rapid changes of dendritic spine morphology (Honkura *et al*, 2008). Latrunculin A-induced F-actin depolymerization (Okamoto *et al*, 2004) or stimulation of n-cofilin activity by inactivation of the negative regulator LIMK-1 leads to shrinkage of spines (Meng *et al*, 2002; Zhou *et al*, 2004). On the contrary, high frequency stimulation of neurons stabilizes F-actin and increases spine volume (Fukazawa *et al*, 2003), similar to what can be observed on deletion of the n-cofilin gene.

The data presented here strongly support the hypothesis that synaptic F-actin levels are a critical determinant of spine size as well as synaptic connectivity. It is conceivable that the increased F-actin levels in n-cof$^{flx/flx,CaMKII\text{-}cre}$ mice can 'freeze' and thereby stabilize synaptic connections *in vivo*, a mechanism, which might contribute to the observed increase in synapse number in mutant mice. Spine morphology is thought to be linked to synaptic plasticity and in hippocampal CA3-CA1 synapses, LTP coincides with an increase in spine size, and LTD was correlated with spine shrinkage (Tada and Sheng, 2006). Changes in spine volume might contribute to spatial restriction of signalling molecules, such as $Ca^{2+}$ (Yuste *et al*, 2000), inducing durable modification of synaptic efficacy (Cingolani and Goda, 2008). However, a direct proof that structural changes are required for synaptic plasticity is difficult (Cingolani and Goda, 2008), particularly in the light of studies, which showed that modification of synaptic physiology and spine morphology can be dissociated under certain conditions (Okamoto *et al*, 2004; Zhou *et al*, 2004; Wang *et al*, 2007).

Here, we show that L-LTP and LTD are altered in the absence of n-cofilin. Interestingly, early LTP does not seem to be affected in n-cof$^{flx/flx,CaMKII\text{-}cre}$ mice. This might reflect the necessity for structural changes in L-LTP and LTD, driven by n-cofilin. Inactivation of LIMK-1 presumably leads to dephosphorylation and activation of n-cofilin, which is accompanied by LTP induction in CA3-CA1 synapses (Meng *et al*, 2002). In addition, LIMK-1 knockout mice (LIMK-1$^{-/-}$) have smaller spine heads. These are opposite effects when compared with n-cof$^{flx/flx,CaMKII\text{-}cre}$ mice. According to the known LIMK-cofilin pathway, the LIMK-1 knockout mice represent a 'gain of function' model and the n-cof$^{flx/flx,CaMKII\text{-}cre}$ mice a 'loss of function' in terms of n-cofilin activity.

However, a number of differences between the two models are difficult to reconcile with such a simple relation. For example the number of synapses was not changed in the LIMK-1 mouse model, whereas n-cof$^{flx/flx,CaMKII\text{-}cre}$ mice have a 50% increase. Second, in n-cof$^{flx/flx,CaMKII\text{-}cre}$ mice, we were not able to induce LTD and rather observed a significant potentiation effect. Neither the LIMK-1$^{-/-}$ model nor *in vitro* studies had earlier suggested a function of n-cofilin in synaptic depression (Zhou *et al*, 2004; Wang *et al*, 2007).

When comparing the LIMK-1$^{-/-}$ model and the n-cof$^{flx/flx,CaMKII\text{-}cre}$ mice, one should be aware that the LIMK-1 studies were performed in a conventional knockout (LIMK-1 was deleted in the entire mouse), whereas in our studies, n-cofilin was specifically removed from principal neurons of the forebrain. The results for n-cofilin are, therefore, uncoupled from any secondary effects of interneurons or glia cells.

The exact molecular mechanism for the potentiation induced in n-cof$^{flx/flx,CaMKII\text{-}cre}$ mice by the LTD protocols is currently unknown. One explanation might be the increased synaptic connectivity, which could protect from LTD. Alternatively, more dynamic mechanisms can influence synaptic plasticity. LTD is thought to result from stimulated loss of AMPAR out of the synaptic domain into the extrasynaptic space, in which receptors are normally cleared by endocytosis. The decreased extrasynaptic AMPAR mobility would diminish the clearance into the extrasynaptic space, whereas the bulk flow of AMPAR to the surface of the synaptic area would increase AMPAR representation and explain the lack of depression and even the mild potentiation as seen in n-cof$^{flx/flx,CaMKII\text{-}cre}$ mice.

Earlier studies had implicated actin remodelling in AMPAR- and NMDAR-dependent synaptic depression (Wang *et al*, 2007), and availability of glutamate receptors, mainly AMPAR at the postsynaptic membrane had been linked to synaptic plasticity (Sheng and Kim, 2002). Mechanistically, the availability of AMPAR in the synapse and hence synaptic transmission can be controlled by exchange of AMPAR between synaptic and extrasynaptic domains through lateral diffusion (Heine *et al*, 2008). Consequently, lateral diffusion of AMPAR might provide an important molecular switch for learning (Triller and Choquet, 2005; Renner *et al*, 2009b).

Hence, it is of considerable interest to understand the exact mechanisms of receptor fencing, and receptor mobility at the postsynaptic membrane. The n-cofilin deletion results in a shift towards a stable F-actin pool in the synapse, and using high-resolution tracking of AMPAR mobility, we observed that such filament stabilization significantly decreased AMPAR mobility. One explanation for these findings would be either a direct interaction of F-actin with the receptor complexes, or a dense cortical actin network, which generally limits the diffusion of integral membrane proteins (Shen *et al*, 2000; Coleman *et al*, 2003). The fencing effect we observed was specific for receptors, as mobility of lipid rafts in the membrane was not altered. Apart from receptor diffusion, delivery and uptake of receptors from the surface can influence synaptic plasticity; however, at this juncture we do not know if n-cofilin has a function in receptor trafficking in the central nervous system.

In conclusion, our data shown here, together with earlier findings provide strong support for a critical function of the actin cytoskeleton in restricting diffusion of postsynaptic receptors, possibly through collision of receptors with F-actin or by directly tethering receptors (Kusumi *et al*, 2005; Renner *et al*, 2008, 2009b). Using actin interfering drugs, both synaptic and extrasynaptic compartments were affected, whereas in n-cofilin mutants only receptor mobility in the extrasynaptic area was decreased. This suggests a complex pattern of controlling AMPAR availability. In the synaptic area, the PSD matrix might be mainly responsible for receptor mobility, whereas receptor diffusion in the extrasynaptic space is possibly ruled by the cortical actin meshwork.

One exciting aspect of n-cofilin modulated synaptic plasticity is how the described differences ultimately impact on complex behaviour such as learning and memory. The molecular alterations in n-cof$^{flx/flx,CaMKII\text{-}cre}$ mice do not seem to have an impact on the working memory and exploratory learning. However, all aspects of associative learning—aversive and reward-based learning—were found to be severely

 

impaired. Unfortunately, we cannot give a conclusive answer on long-term memory, as this requires proper acquisition in first place, which is practically absent in n-cof$^{flx/flx,CaMKII\text{-}cre}$ mice.

The morphological alterations alone are unlikely to account for the deficits described here in n-cof$^{flx/flx,CaMKII\text{-}cre}$ mice. For example, LIMK-1$^{-/-}$ mice have severely altered spine morphology; however, learning is only slightly affected (Meng *et al*, 2002).

In conclusion, our data support the evolving scheme that actin-binding proteins represent a tool box for neurons to introduce specificity in actin-guided synaptic transmission. The n-cofilin uses actin to control spine shape and AMPAR mobility, whereas, for example, the G-actin-binding protein profilin2 regulates presynaptic function and vesicle release (Pilo Boyl *et al*, 2007). The number of examples is growing (Offenhauser *et al*, 2006) and these genetic studies will be crucial for interpreting the true function of actin in the brain. Alterations of actin dynamics might also have a crucial function in various clinical conditions. In human beings for example, changes in n-cofilin activity are thought to contribute to mental disorders (Bamburg and Wiggan, 2002), and deletion of the cofilin regulator LIMK-1 has been linked to Williams' syndrome (Frangiskakis *et al*, 1996). Williams' syndrome patients frequently show mental retardation and a peculiar social behaviour. In this respect, it is interesting that our conditional n-cofilin mouse model shows impaired learning, and that complete deletion of n-cofilin from brain results in severe retardation and a lissencephaly-like phenotype in the mouse (Bellenchi *et al*, 2007).

## Materials and methods

### Mice

Forebrain-specific deletion of n-cofilin was achieved by crossing the conditional n-cofilin allele (n-cof$^{flx/flx}$) (Bellenchi *et al*, 2007) with a transgenic cre-expressing line, driven by CaM-kinase II α-subunit promoter (CaMKII-cre) (Minichiello *et al*, 1999). For imaging studies, a GFP-expressing transgenic line (*Thy1*-GFP-M) (Feng *et al*, 2000) was crossed into the n-cof$^{flx/flx,CaMKII}$ strain. Genotyping of mice was performed by PCR as described in Supplementary data.

### Biochemistry

Tissue extracts from brain were prepared by homogenizing fresh tissues in ice-cold lysis buffer (in mM: 20 Tris–HCl pH 8.0, 100 NaCl, 5 EGTA, 2 EDTA, 0.5% TritonX-100 and EDTA-free protease-inhibitors, Complete, Roche) using a tight fitting Douncer. F/G-actin ratio determination and synaptosome preparation and fractionation are described in Supplementary data.

### Morphology of GFP-expressing mice

After perfusion with 4% PFA/PBS (pH 7.4), brains were postfixed over night in 4% PFA/PBS at 4°C and cut in 100 μm thick transversal sections. Sections were incubated in propidium iodide/PBS (500 nM) (Molecular Probes), washed three times with PBS for 5 min, incubated in 50% glycerol for 10 min and mounted on gelatinized microscope slides in 50% glycerol. Second-order dendritic branches in the *stratum radiatum* of the hippocampal CA1 region were imaged by confocal microscopy (Leica SP5). Z-projections of image stacks were generated by using ImageJ software. MetaMorph imaging software was used for morphometric analysis.

### Electron microscopy

Eight-week-old mice were perfused with 4% PFA/2% glutaraldehyde in phosphate buffer (0.1 M PB, pH 7.4). The brains were postfixed in the same fixative for 4 h, and small specimens taken from the dorsal hippocampus were postfixed in 1% $OsO_4$ in 0.1 cacodylate buffer, dehydrated and embedded in epoxy resin. Serial ultrathin sections were collected on pioloform-coated, single-hole grids, stained with uranyl acetate and lead citrate and observed in a JEM-1010 transmission electron microscope (Jeol) equipped with a side-mounted CCD camera (Mega View III, Soft Imaging System). Spine density was estimated using a physical disector on micrographs of adjacent serial sections taken at $\times 20.000$ ($n = 3$ mice per group). Morphometric analysis was performed on electron micrographs taken at $\times 75000$ using ImageJ. Presynaptic terminals were defined by the presence of at least three vesicles and clear synaptic contacts characterized by a cleft and a well-defined PSD.

### Electrophysiology

Age of the mice used for electrophysiological recordings was between postnatal days 14 and 26 for LTD and between 35 and 46 days for all other experiments. For experimental details, see Supplementary data.

### Behaviour analysis

For all behavioural analyses, age- and sex-matched n-cof$^{flx/flx}$ mice were used as controls. All experimental paradigms including MWM, fear conditioning, Y-maze, hole-board and conditioned place preference are described in detail in Supplementary data.

### Lateral diffusion

*Cell culture.* Generation of hippocampal cultures were preformed essentially as described before (Renner *et al*, 2009a). Briefly, hippocampal neurons from individual embryos at days 16–17 (E16-17) were cultured at a density of $6 \times 10^4$ cells/cm$^2$ on coverslips precoated with 80 μg/ml poly-D,L-ornithine (Sigma Aldrich, Lyon, France) and 5% foetal calf serum (Invitrogen). Cultures were maintained in serum-free Neurobasal medium supplemented with B27 and 2 mM glutamine (Invitrogen). Tail biopsies of dissected embryos were retained for genotyping. For morphometric analysis of dendritic spines, neurons were transfected with GFP using Lipofectamine2000 (Invitrogen) following the instructions of the manufacturer. Dendritic spine width and length was measured by using self-made, MATLAB-based software.

*Single particle tracking.* To track AMPAR movement, QDs conjugated with goat F(ab′)2 anti-rabbit or anti-mouse IgG were coupled to primary antibody directed against AMPAR subunit GluR2. Primary hippocampal cultures (21–24 days *in vitro*, DIV) were incubated for 10 min at 37°C with the pre-coupled QDs. ChTx (Sigma Aldrich) was biotinylated with the EZ-Link Sulfo-NHS-Biotin kit (Pierce, Perbio Science France, Brebières, France). Incubation of neurons with biotinylated ChTX was performed as described before (Renner *et al*, 2009a) Tracking and quantitative analysis was performed as described earlier (Dahan *et al*, 2003; Ehrensperger *et al*, 2007). For details, see Supplementary data.

### Statistical analysis

In all behavioural tests, one-way ANOVA (and in which appropriate, repeated measures ANOVA) was used to assess statistical differences between genotypes or treatment and to check for genotype × treatment interactions. In general, Fisher's PLSD was used as a *post hoc* test given that data were normally distributed and variance was not significantly different for n-cof$^{flx/flx,CaMKII}$ mice and n-cof$^{flx/flx}$ controls. The unpaired two-tailed Student's *t*-test was used when comparing only two sets of data with normal distributions.

### Supplementary data

Supplementary data are available at *The EMBO Journal* Online (http://www.embojournal.org).

## Acknowledgements

We thank Dr JR Sanes for *Thy1*-GFP-M transgenic mice; D Farley, R Migliozzi and K Ociepka for technical support. MBR was supported by a post-doctoral fellowship from the Deutsche Forschungsgemeinschaft (RU-1232/1-1) and by the Stiftung Rheinland-Pfalz (961-386261/877). MR, DC and AT were supported

by grants from Agence National de la Recherche (ANR08-Blan-0282) and Fondation Pierre-Gilles de Gennes. MG was supported by MIUR-PRIN, Regione Piemonte (Ricerca Sanitaria Finalizzata grant no. 142) and Telethon-Italy (grant no. GGP05236A); HV was supported by a fellowship from Secretaría de Estado de Universidades e Investigación, MEC (EX2006-0294). MSP was supported by Compagnia di San Paolo (Torino 2007) and Regione Piemonte (Ricerca Sanitaria Finalizzata 2006 and 2008).

## Conflict of interest

The authors declare that they have no conflict of interest.

## References

Albensi BC, Oliver DR, Toupin J, Odero G (2007) Electrical stimulation protocols for hippocampal synaptic plasticity and neuronal hyper-excitability: are they effective or relevant? *Exp Neurol* **204:** 1–13

Bamburg JR, Wiggan OP (2002) ADF/cofilin and actin dynamics in disease. *Trends Cell Biol* **12:** 598–605

Bellenchi GC, Gurniak CB, Perlas E, Middei S, Ammassari-Teule M, Witke W (2007) N-cofilin is associated with neuronal migration disorders and cell cycle control in the cerebral cortex. *Genes Dev* **21:** 2347–2357

Borgdorff AJ, Choquet D (2002) Regulation of AMPA receptor lateral movements. *Nature* **417:** 649–653

Choquet D, Triller A (2003) The role of receptor diffusion in the organization of the postsynaptic membrane. *Nat Rev Neurosci* **4:** 251–265

Cingolani LA, Goda Y (2008) Actin in action: the interplay between the actin cytoskeleton and synaptic efficacy. *Nat Rev Neurosci* **9:** 344–356

Coleman SK, Cai C, Mottershead DG, Haapalahti JP, Keinanen K (2003) Surface expression of GluR-D AMPA receptor is dependent on an interaction between its C-terminal domain and a 4.1 protein. *J Neurosci* **23:** 798–806

D'Hooge R, De Deyn PP (2001) Applications of the Morris water maze in the study of learning and memory. *Brain Res Rev* **36:** 60–90

Dahan M, Levi S, Luccardini C, Rostaing P, Riveau B, Triller A. (2003) Diffusion dynamics of glycine receptors revealed by single-quantum dot tracking. *Science* **302:** 442–445

Dillon C, Goda Y (2005) The actin cytoskeleton: integrating form and function at the synapse. *Annu Rev Neurosci* **28:** 25–55

Ehrensperger MV, Hanus C, Vannier C, Triller A, Dahan M (2007) Multiple association states between glycine receptors and gephyrin identified by SPT analysis. *Biophys J* **92:** 3706–3718

Feng G, Mellor RH, Bernstein M, Keller-Peck C, Nguyen QT, Wallace M, Nerbonne JM, Lichtman JW, Sanes JR (2000) Imaging neuronal subsets in transgenic mice expressing multiple spectral variants of GFP. *Neuron* **28:** 41–51

Frangiskakis JM, Ewart AK, Morris CA, Mervis CB, Bertrand J, Robinson BF, Klein BP, Ensing GJ, Everett LA, Green ED, Proschel C, Gutowski NJ, Noble M, Atkinson DL, Odelberg SJ, Keating MT (1996) LIM-kinase1 hemizygosity implicated in impaired visuospatial constructive cognition. *Cell* **86:** 59–69

Fukazawa Y, Saitoh Y, Ozawa F, Ohta Y, Mizuno K, Inokuchi K (2003) Hippocampal LTP is accompanied by enhanced F-actin content within the dendritic spine that is essential for late LTP maintenance *in vivo*. *Neuron* **38:** 447–460

Gruart A, Munoz MD, Delgado-Garcia JM (2006) Involvement of the CA3-CA1 synapse in the acquisition of associative learning in behaving mice. *J Neurosci* **26:** 1077–1087

Halpain S (2000) Actin and the agile spine: how and why do dendritic spines dance? *Trends Neurosci* **23:** 141–146

Heine M, Groc L, Frischknecht R, Beique JC, Lounis B, Rumbaugh G, Huganir RL, Cognet L, Choquet D (2008) Surface mobility of postsynaptic AMPARs tunes synaptic transmission. *Science* **320:** 201–205

Honkura N, Matsuzaki M, Noguchi J, Ellis-Davies GC, Kasai H (2008) The subspine organization of actin fibers regulates the structure and plasticity of dendritic spines. *Neuron* **57:** 719–729

Kim CH, Lisman JE (1999) A role of actin filament in synaptic transmission and long-term potentiation. *J Neurosci* **19:** 4314–4324

Kusumi A, Nakada C, Ritchie K, Murase K, Suzuki K, Murakoshi H, Kasai RS, Kondo J, Fujiwara T (2005) Paradigm shift of the plasma membrane concept from the two-dimensional continuum fluid to the partitioned fluid: high-speed single-molecule tracking of membrane molecules. *Annu Rev Biophys Biomol Struct* **34:** 351–378

Matus A (2000) Actin-based plasticity in dendritic spines. *Science* **290:** 754–758

Meberg PJ, Ono S, Minamide LS, Takahashi M, Bamburg JR (1998) Actin depolymerizing factor and cofilin phosphorylation dynamics: response to signals that regulate neurite extension. *Cell Motil Cytoskeleton* **39:** 172–190

Meng Y, Zhang Y, Tregoubov V, Janus C, Cruz L, Jackson M, Lu WY, MacDonald JF, Wang JY, Falls DL, Jia Z (2002) Abnormal spine morphology and enhanced LTP in LIMK-1 knockout mice. *Neuron* **35:** 121–133

Minichiello L, Korte M, Wolfer D, Kuhn R, Unsicker K, Cestari V, Rossi-Arnaud C, Lipp HP, Bonhoeffer T, Klein R (1999) Essential role for TrkB receptors in hippocampus-mediated learning. *Neuron* **24:** 401–414

Offenhauser N, Castelletti D, Mapelli L, Soppo BE, Regondi MC, Rossi P, D'Angelo E, Frassoni C, Amadeo A, Tocchetti A, Pozzi B, Disanza A, Guarnieri D, Betsholtz C, Scita G, Heberlein U, Di Fiore PP (2006) Increased ethanol resistance and consumption in Eps8 knockout mice correlates with altered actin dynamics. *Cell* **127:** 213–226

Okamoto K, Nagai T, Miyawaki A, Hayashi Y (2004) Rapid and persistent modulation of actin dynamics regulates postsynaptic reorganization underlying bidirectional plasticity. *Nat Neurosci* **7:** 1104–1112

Pilo Boyl P, Di Nardo A, Mulle C, Sassoe-Pognetto M, Panzanelli P, Mele A, Kneussel M, Costantini V, Perlas E, Massimi M, Vara H, Giustetto M, Witke W (2007) Profilin2 contributes to synaptic vesicle exocytosis, neuronal excitability, and novelty-seeking behavior. *EMBO J* **26:** 2991–3002

Racz B, Weinberg RJ (2006) Spatial organization of cofilin in dendritic spines. *Neuroscience* **138:** 447–456

Renner M, Choquet D, Triller A (2009a) Control of the postsynaptic membrane viscosity. *J Neurosci* **29:** 2926–2937

Renner M, Specht CG, Triller A (2008) Molecular dynamics of postsynaptic receptors and scaffold proteins. *Curr Opin Neurobiol* **18:** 532–540

Renner ML, Cognet L, Lounis B, Triller A, Choquet D (2009b) The excitatory postsynaptic density is a size exclusion diffusion environment. *Neuropharmacology* **56:** 30–36

Reymann KG, Frey JU (2007) The late maintenance of hippocampal LTP: requirements, phases, 'synaptic tagging', 'late-associativity' and implications. *Neuropharmacology* **52:** 24–40

Shen L, Liang F, Walensky LD, Huganir RL (2000) Regulation of AMPA receptor GluR1 subunit surface expression by a 4. 1N-linked actin cytoskeletal association. *J Neurosci* **20:** 7932–7940

Sheng M, Kim MJ (2002) Postsynaptic signaling and plasticity mechanisms. *Science* **298:** 776–780

Sorra KE, Harris KM (2000) Overview on the structure, composition, function, development, and plasticity of hippocampal dendritic spines. *Hippocampus* **10:** 501–511

Tada T, Sheng M (2006) Molecular mechanisms of dendritic spine morphogenesis. *Curr Opin Neurobiol* **16:** 95–101

Tardin C, Cognet L, Bats C, Lounis B, Choquet D (2003) Direct imaging of lateral movements of AMPA receptors inside synapses. *EMBO J* **22:** 4656–4665

Triller A, Choquet D (2005) Surface trafficking of receptors between synaptic and extrasynaptic membranes: and yet they do move!. *Trends Neurosci* **28:** 133–139

Wang XB, Yang Y, Zhou Q (2007) Independent expression of synaptic and morphological plasticity associated with long-term depression. *J Neurosci* **27:** 12419–12429

Yuste R, Majewska A, Holthoff K (2000) From form to function: calcium compartmentalization in dendritic spines. *Nat Neurosci* **3:** 653–659

Zhou Q, Homma KJ, Poo MM (2004) Shrinkage of dendritic spines associated with long-term depression of hippocampal synapses. *Neuron* **44:** 749–757

 